ORIGINAL RESEARCH

Chinese Herbal Medicine Guilu Erxian Glue Inhibits Osteoclast Formation and Activity via Mc3t3-Derived Extracellular Vesicles in vitro

Yuhao Si, PhD; Shaoshuo Li, PhD; Yang Guo, PhD; Lining Wang, PhD; Yong Ma, PhD; Heng Yin, PhD

ABSTRACT

Background • Osteoporosis is a systemic bone disease characterized by decreased bone density and quality, destruction of bone microstructure, and increased bone fragility. Extracellular vesicles are lipid bilayer nanoparticles that participate in intercellular communication. Extracellular vesicles are becoming popular in the study of osteoporosis and the bone cell microenvironment. Extracellular vesicles can transmit cell signals and regulate bone homeostasis. Our previous studies revealed that the Chinese herbal medicine Guilu Erxian Glue promotes type I collagen synthesis and osteoprotegerin secretion by osteoblasts in rats, reverses the imbalance of bone homeostasis, and alleviates osteoporosis.

Objective • We investigated how osteoblast-derived extracellular vesicles treated with Guilu Erxian Glue affected osteoclasts in vitro.

Methods • We quantified osteoclast differentiation of RAW 264.7 using TRAP staining, cell apoptosis using flow cytometry, extracellular vesicle uptake by fluorescence tracing, bone absorption functions by bone resorption lacuna , and transcription of key genes by quantitative real-time PCR.

Results • Fluorescently labeled mouse preosteoblastic MC3T3-E1 cells secreted nanoscale substances less than 1 μm in diameter. Mouse macrophage RAW 264.7 cells adsorbed these nanoparticles and PKH26-labeled extracellular vesicles derived from MC3T3-E1 cells on the cell membrane surface. Extracellular vesicles from MC3T3-E1 cells treated with Guilu Erxian Glue inhibited the differentiation of osteoclasts induced by receptor activator of nuclear factor-κB ligand and macrophage colony-stimulating factor and reduced the number of lacunae formed by osteoclasts in vitro compared with controls. Extracellular vesicles from MC3T3-E1 cells treated with Guilu Erxian Glue downregulated the relative messenger RNA expression of c-Fos, cathepsin K, nuclear factor of activated T cells 1, and tartrate-resistant acid phosphatase in osteoclasts, which may be part of the mechanism by which they regulate osteoclasts.

Conclusions • Our results demonstrate that extracellular vesicles are essential for signal exchange between osteoblasts and osteoclasts. Although we do not know how Guilu Erxian Glue affects the signaling molecules carried by extracellular vesicles, we have shown for the first time, to our knowledge, that Guilu Erxian Glue can inhibit osteoclast differentiation and function via osteoblast-derived extracellular vesicles. Our findings are conducive to providing a new target for the development of osteoporosis drugs. (*Altern Ther Health Med.* 2023;29(6):400-407).

Yuhao Si, PhD; School of Acupuncture-Moxibustion and Tuina, School of Health Preservation and Rehabilitation, Nanjing University of Chinese Medicine, Nanjing, China; Laboratory for New Techniques of Restoration & Reconstruction of Orthopedics and Traumatology, Nanjing University of Chinese Medicine, Nanjing, China; **Shaoshuo Li**, PhD; **Heng Yin**, PhD; Department of Traumatology & Orthopedics, Wuxi Affiliated Hospital of Nanjing University of Chinese Medicine, Wuxi, China; **Yang Guo**, PhD; Laboratory for New Techniques of Restoration & Reconstruction of Orthopedics and Traumatology, Nanjing University of Chinese Medicine, Nanjing, China; **Lining Wang**, PhD; **Yong Ma**, PhD; Laboratory for New Techniques of Restoration & Reconstruction of Orthopedics and Traumatology, Nanjing University of Chinese Medicine, Nanjing, China; College of Basic Medicine, Nanjing University of Chinese Medicine, Nanjing, China.

Corresponding author: Heng Yin, PhD
E-mail: zhongyiyinheng@126.com

INTRODUCTION

Osteoporosis is a systemic bone disease characterized by decreased bone density and quality, destruction of bone microstructure, and increased bone fragility.[1] The core cause of

osteoporosis is the imbalance between bone resorption and bone formation; specifically, bone resorption is greater than bone formation. Damaged trabecular bone structure decreases bone strength and increases fracture risk. Osteoporosis includes bone loss, postmenopausal osteoporosis, senile osteoporosis, and osteoporotic fracture. According to population statistics, China's population older than 60 years of age has exceeded 210 million people (approximately 15.5% of the total population). The population older than 65 years of age is almost 140 million people (approximately 10.1% of the total population), making China home to the largest population of older people worldwide.[2] Due to China's large population, there is no recent national epidemiological survey. However, an early epidemiological survey from 2006 showed that the prevalence of osteoporosis in people older than 50 years of age in China was approximately 20.7% in women and 14.7% in men. The prevalence of osteoporosis in people older than 60 years of age is significantly higher, especially in women. There were nearly 70 million patients with osteoporosis in China in 2006, and the number of people with bone loss has exceeded 200 million as to 2020. It is speculated that the number of cases of osteoporosis and bone loss in China has far exceeded the above figures.[3] Thus, osteoporosis has become a significant public health issue in China, because of China's increasingly aging population. Moreover, osteoporotic fracture is a major cause of disability and death in older patients. Within 1 year after hip fracture, 20% of patients of all ages die from various complications, and nearly 50% are disabled, with a notable decline in quality of life.[4,5] Moreover, the required treatment and care of patients with osteoporosis and osteoporotic fracture is consuming many of China's human, material, and financial resources, resulting in an increased social burden. The medical expenses for osteoporotic fractures (of the wrist, vertebral body, and hip) in China are projected be as high as $18.9 billion in 2035 and $25.4 billion in 2050.[6]

Guilu Erxian Glue (GEG) is a traditional Chinese herbal medicine that has been widely used in China for hundreds of years for the treatment and prevention of osteoporosis.[7] It contains 4 main ingredients: deer horn, turtle shell, ginseng, and wolfberry. GEG treatment gives minimal side effects[7] and has long-term beneficial effects on aging, perimenopausal syndrome, and degenerative joint disease.[8] In vitro, GEG stimulates the secretion of insulinlike growth factor 1 by osteoblasts and reduces the resorption of osteoclasts.[9] In vivo, GEG suppressed the formation of osteoclasts and bone cavities in rats, and it was shown to reduce joint pain and increase muscle strength in elderly male patients with osteoarthritis of the knee.[10] Notably, GEG prevents and treats bone marrow suppression after cancer chemotherapy.[11] In a previous study, our team found that GEG promoted the synthesis of type I collagen by osteoblasts in rats by upregulation of transforming growth factor β, SMAD3, and phosphorylated SMAD3 in the transforming growth factor β/SMAD3 signaling pathway. [12] The expression of SMAD3 and phosphorylated SMAD3 can stimulate the synthesis of type I collagen by osteoblasts, thus alleviating osteoporosis. We also examined the matrix metallopeptidase 3 (MMP3)/osteopontin/MAPK signaling pathway and found that GEG treatment increased MAPK expression and promoted the secretion of osteoprotegerin by osteoblasts, thus reversing the imbalance of bone formation and bone absorption.[13,14]

Interestingly, recent studies have found that bone remodeling can be regulated by critical factors transported in extracellular vesicles (EVs).[15] EVs can be used to effectively treat pathological bone loss by regulating the bidirectional signal transduction between osteoblasts and osteoclasts.[16] In addition, EVs derived from osteoblasts contain receptor activator of nuclear factor-κB ligand (RANKL) protein, which can activate the RANKL-RANK interaction and lead to the formation of osteoclasts. The communication between osteoblasts and osteoclasts mediated by EVs represents a new bone remodeling mechanism.[17] EVs are bilayer nanovesicles that are grouped into 3 types by their diameter and biological origin: apoptotic bodies (>1000 nm), microvesicles (100-1000 nm), and exosomes (30-100 nm).[18,19] Among them, apoptotic bodies are a product of cell apoptosis . Therefore, research relating to regenerative medicine has mainly focused on microvesicles and exosomes.

Osteoblasts secrete EVs, which carry biological signals that can promote the differentiation of bone marrow mesenchymal stem cells into osteoblasts.[20] MC3T3-E1 is a mouse preosteoblastic cell line often used to study osteoblast physiology and pathology.[21] The similarities of cell expansion, proliferation, and mineralization between primary osteoblasts and MC3T3-E1 cells make this cell line superior to the osteosarcoma cell lines Saos-2 and MG-63. Thus, MC3T3-E1 cells are usually used to simulate the behavior of osteoblasts in osteoporosis research.[22] Ge et al conducted proteomic research on EVs derived from MC3T3-E1 cells (MC3T3-EVs) and identified 1069 proteins involved in the osteogenesis signaling pathway.[23] Cui et al showed that MC3T3-EVs could differentiate the mouse stromal cell line ST2 into osteoblasts, implying that MC3T3-EVs have osteogenic potential.[24] Alfredo et al found that osteoblast EVs are involved in intercellular communication between bone cells, contribute to the RANKL pro-osteoclastic effect, and shuttle antiosteoclast drugs, representing a potential means of targeted therapeutic delivery.[25]

Traditional Chinese medicines, such as GEG, usually treat osteoporosis through multiple targets and pathways.[26] GEG can directly influence osteoblasts and thus facilitate osteogenesis, but it is unclear whether it can exert an antiosteoporotic effect via osteoblast-derived EVs. Thus, in the present work, we treated MC3T3-E1 cells with GEG and monitored the effects of MC3T3-EVs on osteoclast differentiation, apoptosis, and bone resorption function to further clarify the mechanism of GEG in the treatment of osteoporosis.

MATERIALS AND METHODS

Ethics

The Medical Ethics Committee of Nanjing University of Chinese Medicine approved the current study (No. ACU200403). We conducted this study in accordance with the relevant standard guidelines and regulations for animal research.

Preparation of serum from rats treated with GEG or normal saline

We purchased commercially available GEG from the Jiangsu Province Hospital of Traditional Chinese Medicine. Rats purchased from Nanjing Qinglongshan Animal Breeding Farm (license number: SCXK (Zhejiang) 2021-0001) were randomly divided into a GEG group (n = 20) and a control group (n = 10). The body surface area of the rats was used to calculate the doses: the GEG group was orally given 0.23 g GEG once per day for 7 days, and the control group was orally given equivalent saline once per day for 7 days. We anesthetized the rats by intraperitoneal injection of 3% pentobarbital sodium and then drew blood from the abdominal aorta. The blood samples were placed in a high-speed centrifuge at 4°C for 10 minutes (1200 *g*), and the serum supernatant was collected. The serum samples from the rats in the same treatment group were combined, passed through a 0.22 μm filter membrane, and stored at -20°C.

Cell culture and collection of conditioned media containing EVs

RAW 264.7 (SCSP-5036) and MC3T3-E1 subclone 14 (GNM15) cells were purchased from the National Collection of Authenticated Cell Cultures.

The MC3T3-E1 culture medium consisted of 89% Minimum Essential Medium Alpha (α-MEM, Gibco), 10% EV-depleted fetal bovine serum (Shanghai XP Biomed Ltd), and 1% penicillin (Gibco). The medium was changed once every 2 days. When the cell density reached 80%-90% confluence, the cells were subcultured 1:2 or 1:3 by trypsin digestion for 1 minute, followed by gentle mixing, centrifugation, resuspension, and seeding.

To prepare the MC3T3-E1–derived conditioned medium containing EVs, culture medium from MC3T3-E1 cells was collected after 3 passages (approximately the fifth day). The culture medium was centrifuged for 30 minutes at 2000*g* and 4 °C to remove dead cells and cell fragments. We transferred 90% of the supernatant to a new centrifuge tube, and this was centrifuged again for 45 minutes at 12 000g and 4°C to remove large vesicles. The supernatant was filtered through a 0.22 μm filter membrane and collected as conditioned medium containing EVs. To prepare conditioned medium containing EVs from MC3T3-E1 cells treated with GEG (GEG-MC3T3-EVs), MC3T3-E1 cells were cultured to the second generation, the medium was replaced with serum from rats treated with GEG, and the cells were incubated for 24 hours. Afterward, the medium was substituted with EV-depleted fetal bovine serum for another 48 hours. Finally, the culture medium was collected and centrifuged for 30 minutes at 2000*g* and 4°C, 90% of the supernatant was centrifuged again for 45 minutes at 12 000*g* and 4 °C, and the supernatant was filtered through a 0.22 μm filter membrane and collected.

RAW 264.7 cells were cultured in complete medium that contained 88% high-glucose Dulbecco's Modified Eagle Medium (DMEM, Gibco), 10% Australian-origin fetal bovine serum (Gibco), 1% GlutaMAX (Gibco), 1% sodium pyruvate (Gibco), and 1% penicillin (Gibco). The culture medium was refreshed when it appeared slightly yellow in color. We used a cell scraper to subculture cells at 1:4 or 1:5 when the cell confluence reached 70%-80%. The remaining cells were frozen with commercially available cell cryopreservation solution for long-term storage in liquid nitrogen.

Cell proliferation assay of MC3T3-E1 cells exposed to serum from GEG-treated rats

We used a Click-iT EdU assay (Beyotime Biotechnology) to evaluate MC3T3-E1 cell proliferation as a measure of cytotoxicity. MC3T3-E1 cells were cultured in 6-well plates in complete medium (90% α-MEM plus 10% fetal bovine serum) or in α-MEM containing 5%, 10%, 15%, 20%, or 30% serum from GEG-treated rats for 24 or 48 hours. Then, the cells were fixed and permeabilized. The click reaction solution was prepared in accordance with the manufacturer's instructions; 0.5 mL click reaction solution was added to the cells in each well of a 6-well plate, and the plate was gently shaken to ensure the click reaction solution fully contacted the bottom surface. The plates were incubated for 30 minutes at room temperature in a dark environment. After incubation, the click reaction solution was discarded, and the cells were rinsed with deionized water 3 times for 3 minutes each time. Then, we stained the nuclei with 4',6-diamidino-2-phenylindole dye for 5 minutes, discarded the dye solution, washed the cells with deionized water 3 times for 3 minutes each time, and observed the cells under a fluorescence microscope. ImageJ software was used for semiquantitative analysis of the images.

EV isolation and characterization

We used the ultracentrifugation method to isolate MC3T3-EVs.[27] Briefly, the conditioned medium from MC3T3-E1 cells was added in equal volumes to ultracentrifugation tubes. These tubes were centrifuged for 80 minutes in an ultracentrifuge at 110 000 g and 4°C (rotor type 70 Ti, Beckman Coulter). Next, we discarded the supernatant, added 20 mL precooled phosphate-buffered saline (PBS) into each tube, and ultracentrifuged again for 80 minutes at 110 000 *g* and 4°C. Then, we discarded the supernatant and resuspended the pellet in 50 μL PBS. We took 10 μL of the suspension for transmission electron microscope observation and 10 μL for nanoparticle tracking analysis. The rest of the EV suspension was stored in an ultralow-temperature freezer.

Nanoparticle tracking analysis

First, we used standard nanoparticle products to adjust the detection performance of a nano-flow cytometry NanoFCM instrument (NanoFCM Inc). Then, we diluted 10 μL MC3T3-EVs to 30 μL for examination, and the NanoFCM automatically detected the particle size and concentration.

Transmission electron microscopy

We dripped 10 μL MC3T3-EVs onto a copper mesh to precipitate for 1 minute and applied filter paper to absorb the

suspension. Then, we added 10 μL phosphotungstic acid onto the copper mesh to precipitate for 1 minute and used filter paper to absorb the suspension. The sample was dried at room temperature for 5-10 minutes. We used an electron microscope at 80 kV for observation (HT7700, Hitachi) and selected appropriate angles to take images.

Western blot

We used immunoblotting to evaluate the expression of EV protein markers. The following primary antibodies were tested: rabbit anti-CD9 (ab236630, Abcam), rabbit anti-CD63 (ab134045, Abcam), rabbit anti-TSG101 (ab125011, Abcam), and rabbit anti-calnexin (ab133615, Abcam). We used a bicinchoninic acid protein assay kit (Beyotime Biotechnology) to quantify the protein in 100 μL MC3T3-EVs. We heated one-fifth of the sample volume in loading buffer (Beyotime Biotechnology) at 100 °C for 5 minutes to denature the protein. Then, 20 μg samples were separated on a 10% sodium dodecyl sulfate–polyacrylamide gel electrophoresis gel and then transferred to a polyvinylidene fluoride membrane. We blocked the membrane with skim milk and incubated it with the appropriate primary antibody at 4 °C overnight. Next, the membrane was washed and incubated with the appropriate secondary antibody for 1 hour at room temperature. Finally, we rinsed the membrane with PBS and detected the proteins with a chemiluminescence detection system (MilliporeSigma).

EV absorption test

MC3T3-E1 cells were centrifuged at 200*g* for 3 minutes and washed in PBS twice. Then, the cell suspension was labeled with 1 mM PKH26 (Sigma-Aldrich) in a dark environment for 5 minutes and washed twice (5 minutes each with centrifugation) in complete medium (89%α-MEM, 10% fetal bovine serum and 1% penicillin). A Transwell system with a 1 μm pore size was used for culturing PKH26-labeled MC3T3-E1 cells in the upper chamber and unstained RAW 264.7 cells in the lower chamber. MC3T3-E1 cells were plated at $1\times10^6/cm^2$ and RAW 264.7 cells were plated at $1\times10^5/cm^2$. RAW 264.7 cells were treated with 100 ng/mL RANKL and 30 ng/mL macrophage colony-stimulating factor (M-CSF) for osteoclast induction. The cells in the lower chamber were observed using fluorescence microscopy after 24 and 48 hours.

MC3T3-EVs were labeled with 1 mM PKH26 for 5 minutes in a dark environment, rinsed twice with PBS, and resuspended in complete medium. RAW 264.7 cells were labeled with Hoechst 33342 live-cell dye for 10 minutes in a dark environment, rinsed twice with PBS, and then seeded in a 6-well plate. The resuspended PKH26-labeled MC3T3-EVs were added to Hoechst 33342–labeled RAW 264.7 cells. The cells were observed under a fluorescence microscope after 24 and 48 hours.

Stimulation of RAW 264.7 cells with various interventions

RAW 264.7 cells were treated with the following interventions for 48 hours: (*a*) control group, 10% fetal bovine serum + 90% DMEM + 100 ng/mL RANKL + 30 ng/mL M-CSF; (*b*) GEG-containing serum group, 10% GEG-containing serum + 90% DMEM + 100 ng/mL RANKL + 30 ng/mL M-CSF; (*c*) GEG-MC3T3-EV group, 10 μg/mL GEG-MC3T3-EV + 10% fetal bovine serum + 90% DMEM + 100 ng/mL RANKL + 30 ng/mL M-CSF; (*d*) MC3T3-EV group, 10 μg/mL MC3T3-EV + 10% fetal bovine serum + 90% DMEM + 100 ng/mL RANKL + 30 ng/mL M-CSF; (*e*) alendronate sodium (ALN) group, 10^{-8} M ALN + 10% fetal bovine serum + 90% DMEM + 100 ng/mL RANKL + 30 ng/mL M-CSF; and (*f*) GW4869 group (extracellular vesicle inhibitor), 10 μM GW4869 was added into MC3T3-E1 cells for 48 h of incubation. Then, The MC3T3-E1 culture medium was collected and added to the RAW264.7 cell plate, and then 100 ng/mL RANKL and 30 ng/mL M-CSF were added for stimulation for 5 days.

Detection of osteoclast differentiation

RAW 264.7 cells were plated on 6-well plates at $1\times10^5/cm^2$ and cultured in 2 mL complete medium (89%DMEM + 10% FBS + 1% penicilin) with 100 ng/mL RANKL and 30 ng/mL M-CSF for 4 to 5 days. The medium was changed every 2 days, and tartrate-resistant acid phosphatase (TRAP) staining (Wako) was conducted on the fifth day of stimulation. Three fields of vision were randomly selected to acquire images under ×100 magnification using an inverted microscope. We used ImageJ software to perform semiquantitative analysis of the cell fusion areas in the images.

Detection of osteoclast bone resorption function

RAW 264.7 cells were planted in a bone resorption plate (96 wells) with 1000 cells per well. The culture medium was discarded after 5d of intervention, and then the bone resorption plate was rinsed three times using sterile deionized water for 1 minute each. The plate was drained for 30 minutes and placed under an inverted microscope for observation. Three fields of view were randomly selected in each group to record the number of bone resorption lacunas.

Detection of RAW 264.7 apoptosis by flow cytometry

We used a apoptosis kit (Beyotime Biotechnology) to assess cell apoptosis. RAW 264.7 cells were rinsed twice by PBS, scraped off carefully, transferred to a tube and then 500 μL binding buffer and 5 μL annexin V-EGFP were added to the cells. Then, 5 μL propidium iodide was added in the dark for 10 minutes, and the cells were analyzed by flow cytometer (Merck). Data analysis was completed using IDEAS software.

RNA isolation and quantitative real-time polymerase chain reaction

Total RNA and complementary DNA were prepared using the Total RNA Extraction Kit (Solarbio) and UEIris RT Mix with DNase (All-in-One) (UE Landy) in accordance with the manufacturers' instructions. Quantitative real-time polymerase chain reaction was performed using a StepOne Real-Time PCR System (Applied Biosystems). The messenger RNA (mRNA) expression of *MMP9*, *c-Fos*, nuclear factor of activated T cells 1 (*NFATc1*), cathepsin K (*CTSK*), and *TRAP* was calculated relative to that of the housekeeping gene GAPDH.

Statistical analysis

Data are reported as mean (SD). Data analysis was performed using SPSS version 19.0. *t* tests and 1-way analysis of variance were conducted as appropriate, and $P < .05$ was considered statistically significant.

RESULTS

Effect of serum from GEG-treated rats on the activity of MC3T3-E1 cells

We used the Click-iT EdU assay to evaluate the activity of MC3T3-E1 cells cultured in complete medium (α-MEM containing 10% fetal bovine serum) compared with MC3T3-E1 cells cultured in DMEM containing 5%, 10%, 15%, 20%, or 30% GEG-containing serum (Figure 1A). After 24 hours of intervention, the cell activity of MC3T3-E1 cells treated with 30% GEG-containing serum was significantly lower than the cells treated with 10% fetal bovine serum ($P < .05$, Figure 1B). After 48 hours of intervention, the activity of MC3T3-E1 cells treated with 5% GEG-containing serum was significantly lower than the cells treated with 10% fetal bovine serum ($P < .05$, Figure 1B). There were no significant differences between the other groups. As a result, we chose to use cells treated with 10% GEG-containing serum for the follow-up experiments.

Isolation and identification of MC3T3-EVs

Nanoparticle tracking analysis showed the EV mean particle size was 74.75 nm (Figure 1C). The transmission electron microscopy images demonstrated that the EV shapes were complete, nearly spherical, and uniform (Figure 1D). The concentration of MC3T3-EVs using the bicinchoninic acid protein assay kit was 1.106 (0.082) μg/μL. The EVs were positive for CD63, CD9, and TSG101 by Western blot, whereas calnexin staining was negative (Figure 1E). The proportion of particles at 30-150 nm was 97.66%, and the particle concentration was 1.67×10^9/mL (Figure 1F).

MC3T3-EVs were absorbed by RAW 264.7 cells

In the Transwell experiment, round or irregular red fluorescent substances (marked by arrows in Figure 2A), assumed to be the particles secreted by the PKH26-labeled MC3T3-E1 cells in the upper Transwell layer, were observed on RAW 264.7 cell membranes, and the red fluorescent dye clearly outlined the shape of the cell membranes (Figure 2A). The Transwell setup is shown in Figure 2B. Moreover, after PKH26-labeled MC3T3-EVs were added to RAW 264.7 cells, the orange-red EVs tightly surrounded the blue-stained nuclei (Figure 2A). Thus, MC3T3-EVs were successfully absorbed by RAW 264.7 cells.

GEG-MC3T3-EVs inhibited RAW 264.7 osteoclast differentiation

RAW 264.7 cells were stimulated with RANKL and M-CSF for 4 to 5 days. In BC group, GW4869 group and MC3T3-EV group, the cells fused into large multinucleated cells (Figure 2F).TRAP staining showed that their morphology was irregular or oval, with a clear boundary. Hematoxylin staining showed many purple-red nuclei in the cytoplasm. However, we can barely observe the cell fusion in the GEG-containing serum group, GEG-MC3T3-EV group and ALN group. Semiquantitative analysis showed that RAW 264.7 cell osteoclast differentiation induced by RANKL and M-CSF was significantly inhibited by GEG-MC3T3-EVs but not by MC3T3-EVs ($P < .05$, Figure 2G). There were no significant differences between the GEG-MC3T3-EV, GEG-containing

Figure 1. Identification and Characterization of MC3T3-Derived Extracellular Vesicles (MC3T3-EVs). A, 5-Ethynyl-2'-deoxyuridine (EdU) was used to detect the 24-hour cell activity of MC3T3-E1 cells treated with various concentrations of GEG-containing serum. DAPI, 4',6-diamidino-2-phenylindole; FBS, fetal bovine serum; GEG, Guilu Erxian Glue. B, ImageJ was used to semiquantitatively analyze MC3T3-E1 cell activity based on EdU staining areas (1-way analysis of variance). C, Nanoparticle tracking analysis was used to detect the particle size of MC3T3-EVs. D, A representative image of the morphology of EVs as observed by transmission electron microscopy. E, Western blotting was used to test the marker proteins of EVs. F, Nanoparticle tracking analysis was used to detect the concentration of MC3T3-EVs. Data are representative of 3 independent experiments expressed as mean (SD).

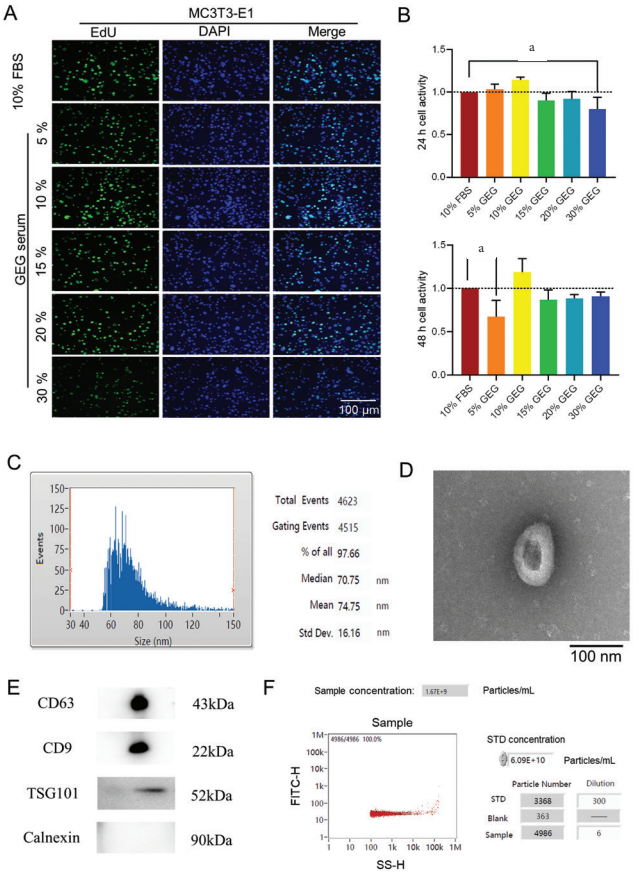

[a]$P < .05$.

Figure 2. Effects of Extracellular Vesicles (EVs) from MC3T3-E1 Cells Treated With Guilu Erxian Glue (GEG) (GEG-MC3T3-EVs) on Osteoclast Differentiation, Resorption, Apoptosis, and Gene Expression. A, The upper panels show the results of the Transwell experiment. The cell membranes of RAW 264.7 cells in the lower layer were dyed red by the particles secreted by the PKH26-labeled MC3T3-E1 cells in the upper layer (the arrows indicate round or irregular red fluorescence substances on RAW 264.7 cell membranes). In the lower panels, PKH26-labeled MC3T3-EVs were added to RAW 264.7 cells. The orange-red EVs attached to the RAW 264.7 cells' nuclei. DAPI, 4',6-diamidino-2-phenylindole. B, Transwell experimental setup. C, Fusion curves of the quantitative real-time polymerase chain reaction experiment. D, Images of bone resorption lacunae (arrows). E, Comparison of the number of bone resorption lacunae. F, Osteoclast differentiation and fusion. G, Semiquantitative analysis of the osteoclast fusion areas. H, Flow cytometry of RAW 264.7 cells. I, Relative messenger RNA expression of matrix metallopeptidase 9 (MMP9), c-Fos, nuclear factor of activated T cells 1 (NFATc1), cathepsin K (CTSK), and tartrate-resistant acid phosphatase (TRAP) in osteoclasts. Glyceraldehyde 3-phosphate dehydrogenase (GAPDH) was used as a control. J, Comparison of apoptosis rates of RAW 264.7 cells. Data are representative of 3 independent experiments expressed as mean (SD). ALN, alendronate sodium.

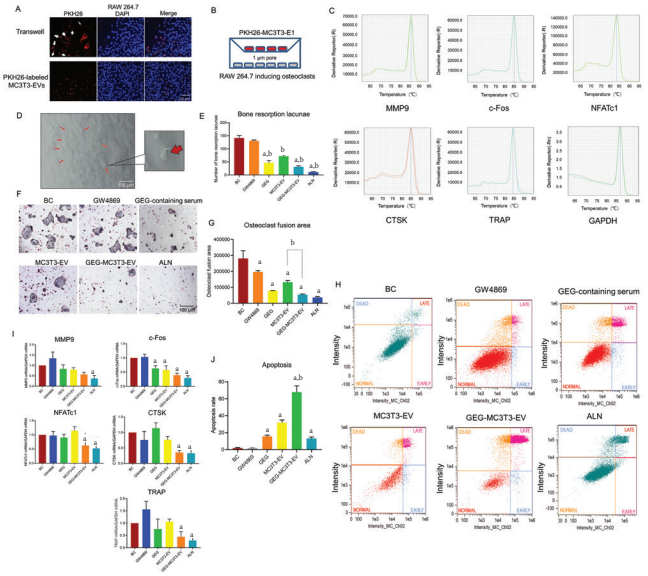

#$P < .05$, vs MC3T3-EV group;
*$P < .05$, vs blank control (BC) group.

serum, and ALN treatment groups for osteoclast differentiation inhibition ($P > .05$, Figure 2G). However, we noticed a trend in the TRAP staining images of weaker inhibition of osteoclast differentiation in the GEG-MC3T3-EV and GEG-containing serum groups than in the ALN group.

GEG-MC3T3-EVs suppressed osteoclast bone resorption

After RAW 264.7 cells were induced and cultured on a bone resorption plate for 4 to 5 days, notable round bone resorption lacunae were observed under an inverted microscope (arrows in Figure 2D). Three visual fields were randomly selected from each group to count the number of bone resorption lacunae. Treatment with GEG-MC3T3-EVs notably reduced the number of bone resorption lacunae formed by osteoclasts compared with the BC group and GW4869 group ($P < .05$, Figure 2E). Its effect was equivalent to that of GEG-containing serum ($P > .05$), superior to that of MC3T3-EVs ($P < .05$), and inferior to that of ALN ($P < .05$, Figure 2E).

GEG-MC3T3-EVs induced RAW 264.7 cell apoptosis

The apoptosis rates in the GEG-MC3T3-EV group, MC3T3-EV group, GEG-containing serum group and ALN group were significantly higher than those in the control group and GW4869 group ($P < .05$), as measured by flow cytometry. Treatment with GEG-MC3T3-EVs had a very significant proapoptotic effect on RAW 264.7 cells, with an apoptosis rate of more than 60%, which was much higher than that in the other groups ($P < .01$, Figure 2H and J).

Detection of osteoclast mRNA expression by real-time reverse transcriptase–polymerase chain reaction

MMP9, *c-Fos*, *NFATc1*, *CTSK*, and *TRAP* were chosen to test mRNA expression (Figure 2C and I). Compared with the control group value of 1.0, the relative mRNA expression in the GEG-MC3T3-EV group was 0.39 for *c-Fos*, 0.63 for *NFATc1*, 0.35 for *CTSK*, and 0.45 for *TRAP* (Figure 2I). The expression of these 4 mRNAs was significantly downregulated (all $P < .05$, Figure 2I). Compared with the control group value of 1.0, the relative mRNA expression in the ALN group was 0.37 for *MMP9*, 0.29 for *c-Fos*, 0.52 for *NFATc1*, 0.32 for *CTSK*, and 0.29 for *TRAP*. The expression of these 5 mRNAs was significantly downregulated (all $P < .05$, Figure 2I). In addition, compared with the control group value of 1.0, the relative mRNA expression of c-Fos was 0.57 in the MC3T3-EV group and 0.63 in the GEG-containing serum group (both $P < .05$, Figure 2I).

DISCUSSION

EVs and their nucleotidase activity were first discovered in 1981. EVs are produced by both normal and tumor cells and play particular physiological and pathological roles in the human body.[28] EVs range in diameter from approximately 100 to 1000 nm and are mainly secreted by plasma membrane shedding and budding. Recent research has focused mainly on exosomes and the function and mechanism of EVs secreted by cultured cells in vitro and in vivo. However, the involvement of EVs in the communication between bone cells remains unclear. Many studies have reported EV production by bone cells, but there are insufficient data on their composition and function.[29] Some EV protein characterization has been reported for osteoblast cell lines, and osteosarcoma cell EVs have been shown to transport osteoclastogenic signals.[30-32] Despite these reports, to date, we know little about the function of EVs in bone biology.

In this study, we adopted a comprehensive method for EV identification, including morphological observation, particle size measurement, and marker protein evaluation, using the "Minimal Information for Studies of Extracellular Vesicles 2018" (MISEV2018) guide.[33] The MC3T3-EVs obtained in our experiment were mostly obvious saucer shaped or large circular shapes under a transmission electron microscope, and the shapes were relatively uniform. The nanoparticle tracking assay results suggested that the diameter of the EVs (mean, 74.75 nm) conforms to the commonly defined range of exosome particle sizes (30-150 nm). CD63 and CD9 are members of transmembrane protein families and are directly involved in sorting EV contents.[34,35] TSG101 is a related protein of the ESCRT (endosomal sorting complexes required for transport) machinery.[36] Calnexin is a protein on the endoplasmic reticulum membrane that is used to distinguish intracellular and extracellular proteins.[37] Our Western blot results revealed that CD9, CD63, and TSG101 were expressed in MC3T3-EVs, whereas calnexin was not, so the MC3T3-EVs met the requirements of EV marker proteins in the MISEV2018 guide.

PKH26 is a fluorescent dye used to label cell membranes by combining with the cell membrane's lipid bilayer. EVs are mainly derived from vesicles formed by lysosome particles. After fusion of the vesicle and receptors on cell membranes, they enter the extracellular matrix. Then, EVs are absorbed by receptors on other cell membranes to play biological roles.[38,39] Our Transwell experiment results demonstrated that PKH26-labeled MC3T3-E1 cells secreted particles that penetrated filter membranes with pores of 1 μm diameter and migrated from the upper layer to the lower layer. Then, those particles combined with the cell membrane of RAW 264.7 cells. We suggest that the PKH26-labeled particles that migrated to the RAW 264.7 cells in the lower layer were probably EVs. Furthermore, we added PKH26-labeled MC3T3-EVs directly onto RAW 264.7 cells and found that those EVs gathered around the nuclei of RAW 264.7 cells, indicating that RAW 264.7 cells had successfully absorbed EVs. Thus, we conclude that RAW 264.7 cells can ingest MC3T3-EVs, which is consistent with previous reports.[25,40]

Under normal circumstances, there is an apparent balance between bone formation and absorption, and the destruction of this balance leads to a pathological state.[41] As an end-stage differentiated cell, osteoclasts cannot be subcultured and can only be cultured and studied in vitro by inducing osteoclast differentiation in precursor cells. The main methods include inducing differentiation of RAW 264.7 cells, bone marrow mononuclear cells, spleen stem cells, and peripheral blood mononuclear cells.[42-44] Currently, most researchers use the RAW 264.7 cell line and bone marrow mononuclear cells. For consistency, we used RAW 264.7 cells, which match the mouse origin of MC3T3-E1 cells, for osteoclast induction. Our purpose was to explore whether GEG can influence osteoclasts and osteoclast precursor cells through MC3T3-EVs. We used RANKL and M-CSF to stimulate RAW 264.7 cells to differentiate into osteoclasts. TRAP staining and semiquantitative analysis showed that GEG-MC3T3-EVs could significantly inhibit the differentiation of osteoclasts, and the inhibitory effect was similar to that of GEG-containing serum and ALN. MC3T3-EVs also had an inhibitory effect on osteoclast differentiation, unlike the control group. However, its effect was weaker than that of GEG-MC3T3-EVs, suggesting that GEG can suppress osteoclast differentiation via EV-mediated intercellular communication. In addition, we found that RAW 264.7 cells formed many round cavities on a bone absorption plate after 4 days of induction, a measure of bone resorption. MC3T3-EVs, GEG-containing serum, GEG-MC3T3-EVs, and ALN significantly inhibited osteoclast bone resorption. ALN produced the strongest effect, followed by GEG-MC3T3-EVs and GEG-containing serum. In the apoptosis experiment of RAW 264.7 cells, GEG-MC3T3-EVs had a potent proapoptotic effect, with an apoptosis rate of more than 60%. This finding implies that GEG can exert a proapoptotic effect on RAW 264.7 cells by affecting MC3T3-EVs and intercellular communication. These results demonstrate that MC3T3-EVs treated with GEG inhibited osteoclast differentiation and bone resorption and promoted osteoclast precursor apoptosis. However, MC3T3-EVs had a weak inhibitory effect on osteoclast differentiation and bone resorption, which was different from previous reports. For instance, primary osteoblast-derived EVs shuttle RANKL to promote osteoclast differentiation and maturation.[25] There have only been a few studies on MC3T3-EVs. Wang et al found that MC3T3-derived exosomes exposed to prolonged tension stimulation promoted osteoclast differentiation and bone resorption.[40] We speculate that the EV isolation method might have influenced these results. The cell supernatant used in the current study underwent 2 centrifugations of 80 minutes each at 110 000*g*, whereas Wang et al only centrifuged the supernatant at 110 000*g* once for 30 minutes. A short centrifugation time probably led to unnecessary impurities in the EV suspension, thus interfering with the final results.[40] Hence, the role of MC3T3-EVs in osteoclast differentiation and maturation requires further study.

The expression of NFATc1 plays a critical role in osteoclast differentiation.A study demonstrated that the differentiation of osteoclasts in NFATc1-knockout mice was significantly inhibited and resulted in osteosclerosis.[45] Additionally, nuclear factor-κB and activator protein 1 are essential downstream targets of the RANK/RANKL/osteoprotegerin pathway. The activation of the activator protein 1 transcription factors Fos, Jun, and activating transcription factor requires the fusion protein c-Fos.[46] Similarly, c-Fos–knockout mice also have obvious osteosclerosis.[46] CTSK and TRAP are both signaling molecules of late osteoclast differentiation and are commonly used markers of bone resorption and osteoclast differentiation.[47] We observed that GEG-MC3T3-EVs significantly reduced the mRNA expression of c-Fos, NFATc1, CTSK, and TRAP compared with that in the control group. This result suggests that the inhibitory effect of GEG-MC3T3-EVs on osteoclast differentiation is related to the downregulation of the RANK/RANKL/osteoprotegerin downstream signaling pathway. However, the underlying mechanism remains to be further explored.

CONCLUSIONS

Unsurprisingly, MC3T3-EVs can promote osteoblast differentiation because MC3T3-E1 cells are osteoblast precursors.[48] However, our study found that MC3T3-EVs significantly inhibited the differentiation and maturation of osteoclasts after GEG treatment. Although we still do not know how GEG changes the signaling molecules carried in MC3T3-EVs, to the best of our knowledge, this is the first study to show that a traditional Chinese medicine formula can directly inhibit osteoclast differentiation and function via EVs. Future research could use high-throughput sequencing to identify differentially expressed RNAs in MC3T3-EVs with and without GEG treatment. Then, experiments would be needed to verify and further clarify how GEG plays an antiosteoporosis role through the exosome pathway. To conclude, osteoblast-derived EVs have the potential to become drug carriers and targets for traditional Chinese medicine in the treatment of osteoporosis, and further research is necessary.

DATA AVAILABILITY STATEMENT

The raw data supporting the conclusions of this article will be made available by the authors upon request.

ETHICS STATEMENT

The animal experiment in this study was reviewed and approved by the Medical Ethics Committee of Nanjing University of Chinese Medicine.

AUTHOR CONTRIBUTIONS

YS, SL, and HY designed and conducted the experiments, collected data, analyzed the data, and wrote the manuscript; YG, YM, and HY conceived and designed this study, supervised the work, and assisted with writing, reviewing, and editing of the manuscript and funding acquisition. All authors have approved the final version of the manuscript.

FUNDING

This study is supported by the National Natural Science Foundation of China (No. 81973878) and is a project funded by the Jiangsu CM Clinical Innovation Center of Degenerative Bone & Joint Disease.

ACKNOWLEDGEMENTS

We wish to thank Dr. Zhao Min for her invaluable assistance with the apoptosis analysis.

CONFLICT OF INTEREST

The authors declare that the research was conducted in the absence of any commercial or financial relationships that could be construed as a potential conflict of interest.

REFERENCES

1. LeBoff MS, Greenspan SL, Insogna KL, et al. The clinician's guide to prevention and treatment of osteoporosis. *Osteoporos Int*. 2022;33(10):2049-2102. doi:10.1007/s00198-021-05900-y
2. Han X, Wei C, Cao GY. Aging, generational shifts, and energy consumption in urban China. *Proc Natl Acad Sci USA*. 2022;119(37):e2210853119. doi:10.1073/pnas.2210853119
3. Liu JM, Zhu DL, Mu YM, Xia WB; Chinese Society of Osteoporosis and Bone Mineral Research, the Chinese Society of Endocrinology, Chinese Diabetes Society, Chinese Medical Association; Chinese Endocrinologist Association, Chinese Medical Doctor Association. Management of fracture risk in patients with diabetes-Chinese Expert Consensus. *J Diabetes*. 2019;11(11):906-919. doi:10.1111/1753-0407.12962
4. Osnes EK, Lofthus CM, Meyer HE, et al. Consequences of hip fracture on activities of daily life and residential needs. *Osteoporos Int*. 2004;15(7):567-574. doi:10.1007/s00198-003-1583-0
5. Keene GS, Parker MJ, Pryor GA. Mortality and morbidity after hip fractures. *BMJ*. 1993;307(6914):1248-1250. doi:10.1136/bmj.307.6914.1248
6. Si L, Winzenberg TM, Jiang Q, Chen M, Palmer AJ. Projection of osteoporosis-related fractures and costs in China: 2010-2050. *Osteoporos Int*. 2015;26(7):1929-1937. doi:10.1007/s00198-015-3093-2
7. Long L, Soeken K, Ernst E. Herbal medicines for the treatment of osteoarthritis: a systematic review. *Rheumatology (Oxford)*. 2001;40(7):779-793. doi:10.1093/rheumatology/40.7.779
8. Tsai CC, Chou YY, Chen YM, Tang YJ, Ho HC, Chen DY. Effect of the herbal drug guilu erxian jiao on muscle strength, articular pain, and disability in elderly men with knee osteoarthritis. *Evid Based Complement Alternat Med*. 2014;2014:297458. doi:10.1155/2014/297458
9. Zhang Y, Mao C, Yan W, Zheng X. Application of cell engineering of herbal Medicine treating bone resorption of osteoclasts. *Conf Proc IEEE Eng Med Biol Soc*. 2005;2005:4958-4961.
10. Chou YJ, Chuu JJ, Peng YJ, et al. The potent anti-inflammatory effect of Guilu Erxian Glue extracts remedy joint pain and ameliorate the progression of osteoarthritis in mice. *J Orthop Surg Res*. 2018;13(1):259. doi:10.1186/s13018-018-0967-y
11. Tian H, Qin W, Wu W, et al. Effects of traditional Chinese medicine on chemotherapy-induced myelosuppression and febrile neutropenia in breast cancer patients. *Evid Based Complement Alternat Med*. 2015;2015:736197. doi:10.1155/2015/736197
12. Zhe Q, Jianwei W, Heng Y, et al. Study on the mechanism of guilu erxian gum in treating osteoporosis. *Chinese Journal of Traditional Chinese Medicine*. 2017;35(4):1008-1013.
13. Yin H, Wang J, Wu M, Ma Y, Wang S, Su Q. Preventive effects of evodiamine on dexamethasone-induced osteoporosis in zebrafish. *BioMed Res Int*. 2019;2019:5859641. doi:10.1155/2019/5859641
14. Yin H, Wang S, Zhang Y, Wu M, Wang J, Ma Y. Zuogui Pill improves the dexamethasone-induced osteoporosis progression in zebrafish larvae. *Biomed Pharmacother*. 2018;97:995-999. doi:10.1016/j.biopha.2017.11.029
15. Behera J, Tyagi N. Exosomes: mediators of bone diseases, protection, and therapeutics potential. *Oncoscience*. 2018;5(5-6):181-195. doi:10.18632/oncoscience.421
16. Yin P, Lv H, Li Y, Deng Y, Zhang L, Tang P. Exosome-mediated genetic information transfer, a missing piece of osteoblast-osteoclast communication puzzle. *Front Endocrinol (Lausanne)*. 2017;8:336. doi:10.3389/fendo.2017.00336
17. Yuan FL, Wu QY, Miao ZN, et al. Osteoclast-derived extracellular vesicles: novel regulators of osteoclastogenesis and osteoclast-osteoblasts communication in bone remodeling. *Front Physiol*. 2018;9:628. doi:10.3389/fphys.2018.00628
18. Ha D, Yang N, Nadithe V. Exosomes as therapeutic drug carriers and delivery vehicles across biological membranes: current perspectives and future challenges. *Acta Pharm Sin B*. 2016;6(4):287-296. doi:10.1016/j.apsb.2016.02.001
19. Raposo G, Stoorvogel W. Extracellular vesicles: exosomes, microvesicles, and friends. *J Cell Biol*. 2013;200(4):373-383. doi:10.1083/jcb.201211138
20. Yang S, Zhu B, Yin P, et al. Integration of human umbilical cord mesenchymal stem cells-derived exosomes with hydroxyapatite-embedded hyaluronic acid-alginate hydrogel for bone regeneration. *ACS Biomater Sci Eng*. 2020;6(3):1590-1602. doi:10.1021/acsbiomaterials.9b01363
21. Wang D, Christensen K, Chawla K, Xiao G, Krebsbach PH, Franceschi RT. Isolation and characterization of MC3T3-E1 preosteoblast subclones with distinct in vitro and in vivo differentiation/mineralization potential. *J Bone Miner Res*. 1999;14(6):893-903. doi:10.1359/jbmr.1999.14.6.893
22. Czekanska EM, Stoddart MJ, Ralphs JR, Richards RG, Hayes JS. A phenotypic comparison of osteoblast cell lines versus human primary osteoblasts for biomaterials testing. *J Biomed Mater Res A*. 2014;102(8):2636-2643. doi:10.1002/jbm.a.34937
23. Ge M, Ke R, Cai T, Yang J, Mu X. Identification and proteomic analysis of osteoblast-derived exosomes. *Biochem Biophys Res Commun*. 2015;467(1):27-32. doi:10.1016/j.bbrc.2015.09.135
24. Cui Y, Luan J, Li H, Zhou X, Han J. Exosomes derived from mineralizing osteoblasts promote ST2 cell osteogenic differentiation by alteration of microRNA expression. *FEBS Lett*. 2016;590(1):185-192. doi:10.1002/1873-3468.12024
25. Cappariello A, Loftus A, Muraca M, Maurizi A, Rucci N, Teti A. Osteoblast-derived extracellular vesicles are biological tools for the delivery of active molecules to bone. *J Bone Miner Res*. 2018;33(3):517-533. doi:10.1002/jbmr.3332
26. Han J, Wan M, Ma Z, Hu C, Yi H. Prediction of targets of curculigoside A in osteoporosis and rheumatoid arthritis using network pharmacology and experimental verification. *Drug Des Devel Ther*. 2020;14:5235-5250. doi:10.2147/DDDT.S282112
27. Shelke GV, Lässer C, Gho YS, Lötvall J. Importance of exosome depletion protocols to eliminate functional and RNA-containing extracellular vesicles from fetal bovine serum. *J Extracell Vesicles*. 2014;3(1):24783. doi:10.3402/jev.v3.24783
28. Trams EG, Lauter CJ, Salem N Jr, Heine U. Exfoliation of membrane ecto-enzymes in the form of micro-vesicles. *Biochim Biophys Acta*. 1981;645(1):63-70. doi:10.1016/0005-2736(81)90512-5
29. Kamel-ElSayed SA, Tiede-Lewis LM, Lu Y, Veno PA, Dallas SL. Novel approaches for two and three dimensional multiplexed imaging of osteocytes. *Bone*. 2015;76:129-140. doi:10.1016/j.bone.2015.02.011
30. Morhayim J, van de Peppel J, Demmers JAA, et al. Proteomic signatures of extracellular vesicles secreted by nonmineralizing and mineralizing human osteoblasts and stimulation of tumor cell growth. *FASEB J*. 2015;29(1):274-285. doi:10.1096/fj.14-261404
31. Nair R, Santos L, Awasthi S, et al. Extracellular vesicles derived from preosteoblasts influence embryonic stem cell differentiation. *Stem Cells Dev*. 2014;23(14):1625-1635. doi:10.1089/scd.2013.0633
32. Garimella R, Washington L, Isaacson J, et al. Extracellular membrane vesicles derived from 143B osteosarcoma cells contain pro-osteoclastogenic cargo: a novel communication mechanism in osteosarcoma bone microenvironment. *Transl Oncol*. 2014;7(3):331-340. doi:10.1016/j.tranon.2014.04.011
33. Théry C, Witwer KW, Aikawa E, et al. Minimal information for studies of extracellular vesicles 2018 (MISEV2018): a position statement of the International Society for Extracellular Vesicles and update of the MISEV2014 guidelines. *J Extracell Vesicles*. 2018;7(1):1535750. doi:10.1080/20013078.2018.1535750
34. Escola JM, Kleijmeer MJ, Stoorvogel W, Griffith JM, Yoshie O, Geuze HJ. Selective enrichment of tetraspan proteins on the internal vesicles of multivesicular endosomes and on exosomes secreted by human B-lymphocytes. *J Biol Chem*. 1998;273(32):20121-20127. doi:10.1074/jbc.273.32.20121
35. Hemler ME. Tetraspanin proteins mediate cellular penetration, invasion, and fusion events and define a novel type of membrane microdomain. *Annu Rev Cell Dev Biol*. 2003;19(1):397-422. doi:10.1146/annurev.cellbio.19.111301.153609
36. Nabhan JF, Hu R, Oh RS, Cohen SN, Lu Q. Formation and release of arrestin domain-containing protein 1-mediated microvesicles (ARMMs) at plasma membrane by recruitment of TSG101 protein. *Proc Natl Acad Sci USA*. 2012;109(11):4146-4151. doi:10.1073/pnas.1200448109
37. Wijenayake S, Eisha S, Tawhidi Z, et al. Comparison of methods for pre-processing, exosome isolation, and RNA extraction in unpasteurized bovine and human milk. *PLoS One*. 2021;16(9):e0257633. doi:10.1371/journal.pone.0257633
38. White IJ, Bailey LM, Aghakhani MR, Moss SE, Futter CE. EGF stimulates annexin 1-dependent inward vesiculation in a multivesicular endosome subpopulation. *EMBO J*. 2006;25(1):1-12. doi:10.1038/sj.emboj.7600759
39. Möbius W, Ohno-Iwashita Y, van Donselaar EG, et al. Immunoelectron microscopic localization of cholesterol using biotinylated and non-cytolytic perfringolysin O. *J Histochem Cytochem*. 2002;50(1):43-55. doi:10.1177/002215540205000105
40. Wang W, Qiao SC, Wu XB, et al. Circ_0008542 in osteoblast exosomes promotes osteoclast-induced bone resorption through m6A methylation. *Cell Death Dis*. 2021;12(7):628. doi:10.1038/s41419-021-03915-1
41. Yin X, Zhou C, Li J, et al. Autophagy in bone homeostasis and the onset of osteoporosis. *Bone Res*. 2019;7(1):28. doi:10.1038/s41413-019-0058-7
42. Boraschi-Diaz I, Komarova SV. The protocol for the isolation and cryopreservation of osteoclast precursors from mouse bone marrow and spleen. *Cytotechnology*. 2016;68(1):105-114. doi:10.1007/s10616-014-9759-3
43. Kong L, Smith W, Hao D. Overview of RAW264.7 for osteoclastogensis study: phenotype and stimuli. *J Cell Mol Med*. 2019;23(5):3077-3087. doi:10.1111/jcmm.14277
44. Faust J, Lacey DL, Hunt P, et al. Osteoclast markers accumulate on cells developing from human peripheral blood mononuclear precursors. *J Cell Biochem*. 1999;72(1):67-80. doi:10.1002/(SICI)1097-4644(19990101)72:1<67::AID-JCB8>3.0.CO;2-A
45. Aliprantis AO, Ueki Y, Sulyanto R, et al. NFATc1 in mice represses osteoprotegerin during osteoclastogenesis and dissociates systemic osteopenia from inflammation in cherubism. *J Clin Invest*. 2008;118(11):3775-3789. doi:10.1172/JCI35711
46. Caputto BL, Cardozo Gizzi AM, Gil GA. c-Fos: an AP-1 transcription factor with an additional cytoplasmic, non-genomic lipid synthesis activation capacity. *Biochim Biophys Acta*. 2014;1841(9):1241-1246. doi:10.1016/j.bbalip.2014.05.007
47. Song F, Zhou L, Zhao J, et al. Eriodictyol inhibits RANKL-induced osteoclast formation and function via inhibition of NFATc1 activity. *J Cell Physiol*. 2016;231(9):1983-1993. doi:10.1002/jcp.25304
48. Holkar K, Kale V, Ingavle G. Hydrogel-assisted 3D model to investigate the osteoinductive potential of MC3T3-derived extracellular vesicles. *ACS Biomater Sci Eng*. 2021;7(6):2687-2700. doi:10.1021/acsbiomaterials.1c00386